European Journal of Pharmaceutical Sciences 195 (2024) 106731

Contents lists available at ScienceDirect

European Journal of Pharmaceutical Sciences

journal homepage: www.elsevier.com/locate/ejps

Solubility of *digitoxin* in supercritical CO_2: Experimental study and modeling

Mohammadreza Sheikhi-Kouhsar [a], Hamidreza Bagheri [b,*], Fahad Alsaikhan [c,d], Ahmed Khalid Aldhalmi [e], Hanan Hassan Ahmed [f]

[a] Department of Chemical Engineering, School of Chemical and Petroleum Engineering, Shiraz University, 71946-84334 Shiraz, Iran
[b] Department of Chemical Engineering, Faculty of Engineering, Shahid Bahonar University of Kerman, 76188-68366 Kerman, Iran
[c] College of Pharmacy, Prince Sattam Bin Abdulaziz University, Al-Kharj 11942, Saudi Arabia
[d] School of Pharmacy, Ibn Sina National College for Medical Studies, Jeddah, Saudi Arabia
[e] College of Pharmacy, Al-Mustaqbal University, 51001 Babylon, Iraq
[f] Department of Pharmacy, Al-Noor University College, Nineveh, Iraq

ARTICLE INFO

Keywords:
Digitoxin
Drug
Semi-empirical correlation
Solubility
sPC-SAFT
SRK
Supercritical CO_2

ABSTRACT

In this communication, the solubility of *digitoxin* drug in supercritical CO_2 was studied at different operating conditions ($311 < T$ (K) < 343, $120 < P$ (bar) < 300). The results revealed *digitoxin* drug solubility (in mole fraction) was between 0.095×10^{-5} to 1.12×10^{-5}. In the case of thermodynamic solubility modeling, cubic and non-cubic equation of states i.e. SAFT (statistical associating fluid theory), SRK (Soave-Redlich-Kwong) and sPC-SAFT (simplified perturbed chain SAFT) EoSs and six density-based correlations (Chrastil, Kumar-Johnston (KJ), Mendez-Santiago-Teja (MST), Garlapati and Madras (GM), Bartle et al. and Sung-Shim models) were considered. All used equations indicated reasonable behavior with appropriate accuracy for the solubility of the *digitoxin* drug. Meanwhile, sPC-SAFT EoS and Kumar-Johnston correlation with AARD% set to 8.96 % and 6.25 %, respectively exhibited greater accuracy in fitting the solubility data. Moreover, total, solvation and vaporization enthalpies of the *digitoxin*/supercritical carbon dioxide binary mixture were calculated based on KJ, Chrastil and Bartle et al. models.

1. Introduction

Carbon dioxide (CO_2) is a greenhouse gas that contributes to climate change. It is produced from burning fossil fuels and makes up 76 % of global greenhouse gas emissions (Oparin et al., 2020; Long et al., 2019). The current level of in the atmosphere is 410 ppm. To address this issue, we need to improve knowledge that can capture or use carbon dioxide (Sodeifian et al., 2024; Soleymani et al., 2023; Bagheri et al., 2021). Supercritical fluids (SCFs) are substances that are at extremely high temperatures and pressures. They exist in a state where there is no clear distinction between liquid and gas. Supercritical CO_2 (SC—CO_2) and water are the most commonly studied SCFs (Khodov et al., 2023; Wang et al., 2023; Bagheri et al., 2019; Asar et al., 2020). They can be used as alternatives to solvents in chemical processes and for environmental cleanup. SC—CO_2 refers to carbon dioxide that is above its critical temperature and pressure (Wang et al., 2023; Bagheri et al., 2019). CO_2 can exist in a supercritical state at certain temperature and pressure conditions ($T_c = 304.25$ K, $P_c = 73.80$ bar). It has a lower critical point compared to other compounds. CO_2 is readily available due to its high concentration in the atmosphere from industrial activities. This makes it useful for various industrial applications. In normal conditions, CO_2 is a gas or a solid called dry ice. However, under supercritical conditions, it has properties of both a gas and a liquid. SC—CO_2 is used in various industries for processes such as food extractions and pharmaceutical applications (Asar et al., 2020; Karn et al., 2013; Bian et al., 2016).

Supercritical substances have both gas and liquid properties, making them useful for various industries (Bagheri et al., 2021). SCFs have been found to be a viable means of processing various substances, including organometallic compounds, monomers, dyes, bioactive compounds, and drugs. Consequently, the application of this technology has extended to multiple industrial sectors (Bagheri et al., 2021; Rezaei et al., 2022; Bagheri et al., 2021). Among all, we considered the application of SC—CO_2 in the pharmaceutical industry (Pan et al., 2022; Shen et al., 2023; Xiang et al., 2023; Li et al., 2019). The much of the newly

* Corresponding author.
E-mail address: hbagheri@uk.ac.ir (H. Bagheri).

https://doi.org/10.1016/j.ejps.2024.106731
Received 26 September 2023; Received in revised form 5 February 2024; Accepted 19 February 2024
Available online 20 February 2024

Table 1
The properties of all used substances (H Bagheri et al., 2021; Sodeifian et al., 2023, https://webbook.nist).

Name	Formula	CAS number	T_m (K)	M_w	Supplier	Purity*
Digitoxin	$C_{41}H_{64}O_{13}$	71–63–6	528	764.94	Jalinous Pharmaceutical Co. Tehran, Iran	99.90 %
Ketoprofen	$C_{16}H_{14}O_3$	38,194–50–2	367–370	254.29	Jalinous Pharmaceutical Co. Tehran, Iran	99.90 %
Carbon dioxide	CO_2	124–38–9	–	44.01	Havaie Pak Tabiat Industrial Gas Co. Kerman, Iran	99.99 %
Methanol	CH_3OH	67–56–1	–	32.04	Merck Co. Germany	99.90 %

* Mass fraction purity (As stated by the supplier).

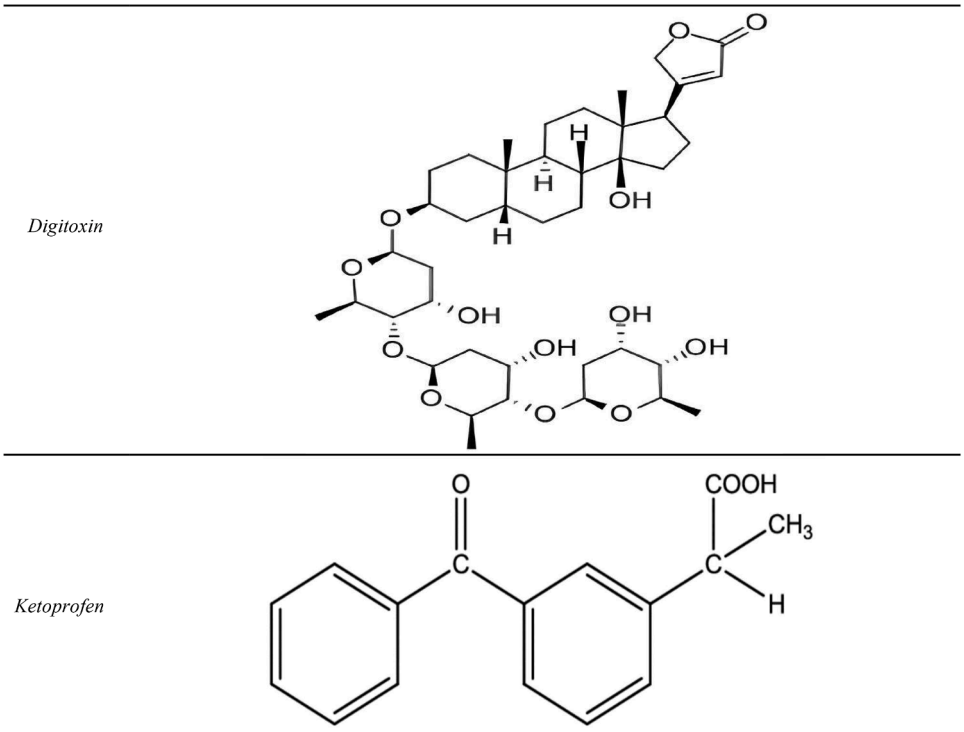

Fig. 1. The structures of drugs in the present investigation.

discovered drugs, have poor solubility in water. Commonly, poor permeability and low aqueous solubility are key reasons for usage of high dosage of poorly water-soluble drug. One of the main challenges in the pharmaceutical industry is creating drugs that can dissolve easily in water and be easily absorbed by the body. To overcome this challenge, new techniques are needed (Xiang et al., 2023; Li et al., 2019; Yi et al., 2018; Su et al., 2023; He et al., 2023; Liu et al., 2023; Jiang and Yan, 2021). Reducing the drug particle size has been introduced as one of the more practical procedures (Knez et al., 2014; Bagheri et al., 2022; López-Periago et al., 2009). So, producing fine solid particles by a process based on an SCFs has received great attention. Various techniques are recommended based on SCF technology to reduce the particle size of drugs and increase the drug solubility. The drug solubility is the main factor to select a desired technique (Soleymani et al., 2023; Sabegh et al., 2012). Consequently, determining the drug solubility of in SCFs and in various circumstances is very important to design processes for a drug applicant (Bagheri et al., 2019; Bagheri et al., 2019).

Supercritical fluids, such as supercritical CO_2, are being applied as an alternative to conventional methods of drug processing in the field of drug delivery. These fluids have been found to be effective and provide a clean way to control the shape, size, and release of drug particles (Karn et al., 2013; Sodeifian et al., 2023). Various techniques using supercritical fluids have been developed for micronizing drug particles, particularly for drugs that are not easily soluble in water. Understanding the solubility behavior of drugs in SCFs is crucial for the production and purification of pharmaceuticals. Therefore, studying the phase behavior of drugs with supercritical fluids is an important first step in drug delivery using these techniques (Bagheri et al., 2021; Bagheri et al., 2019). Measurement of experimental solubility of drugs in SC—CO_2 is very valuable, however, this process is a complex, costly, and time-consuming task, which requests to be substituted by other methods like thermodynamic models. Consequently, different theoretical procedures have been presented for measurement the drugs solubility in the SC—CO_2 (Long et al., 2019; Bagheri et al., 2021). Molecular dynamics simulations, intelligent methods, semi-empirical models, activity coefficient models, and cubic/non-cubic equations of state (EoS) are the most common methods used for theoretical calculation of drugs solubility in the SC—CO_2 (Bagheri et al., 2021; Bagheri et al., 2019). Of course, the appropriate model for prediction the drug solubility in supercritical CO_2 should be determined by a comparison between the experimental solubility data and the computed data by the used thermodynamic model. Peng-Robinson (PR) EoS and Soave-Redlich-Kwong (SRK) EoS as CEoS and SAFT (statistical associating fluid theory) family EoSs as non-CEoS are the most common EoS to predict drug solubility data. Also, many reports have presented various forms of semi-empirical correlations referring to relationships between the operational temperature, pressure, density of supercritical CO_2, and the drugs solubility (Delma et al., 2023; Bagheri et al., 2018). Semi-empirical models are simple correlations, which have indicated satisfactory resultants for modeling the solubility of various drugs in SC—CO_2. The EoSs are more complex in comparison with the semi-empirical correlations, due to EoSs need the thermodynamic properties of both drug and SCF that are

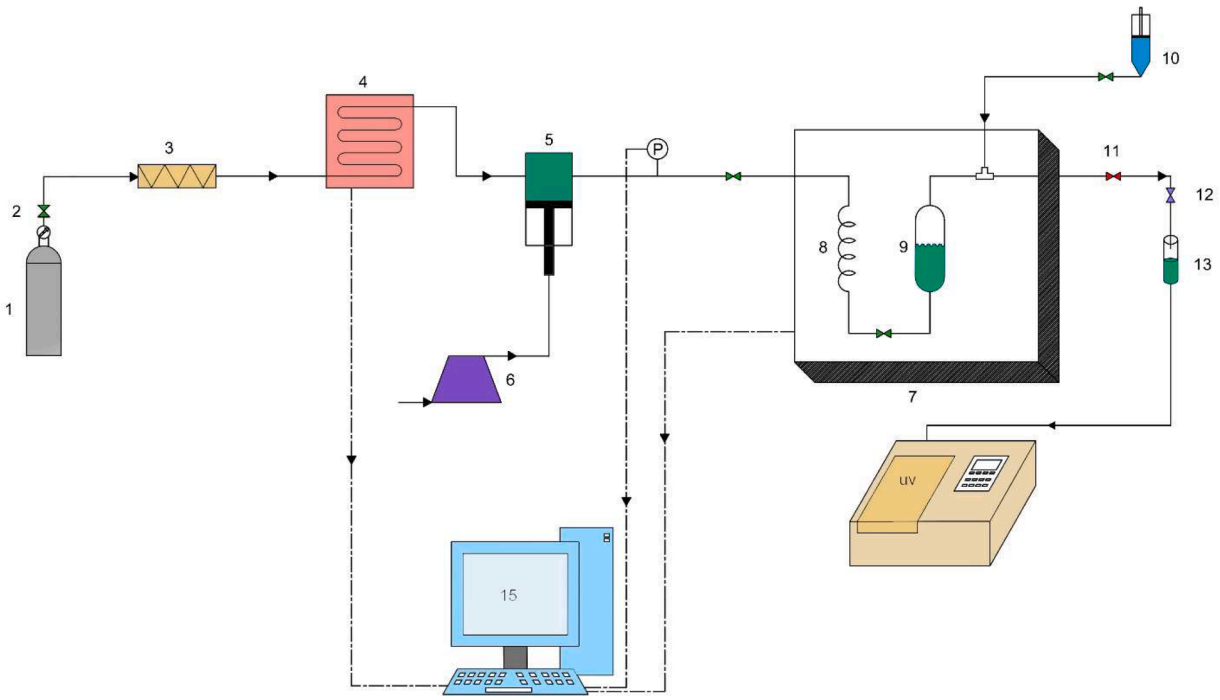

Fig. 2. The schematic of the laboratory setup for *digitoxin* solubility measurement.

Table 2
The *ketoprofen* solubility in SC—CO_2.

T (K)	P (bar)	Literature (Li et al., 2019)	This study	SD × 10^6*	RSD *	AARD**
318.15	200	6.58×10^{-5}	6.54×10^{-5}	0.36	0.55	0.60
318.15	280	9.01×10^{-4}	8.95×10^{-4}	6.70	0.74	0.66
328.15	200	1.16×10^{-4}	1.13×10^{-4}	2.99	2.64	2.58
328.15	240	1.75×10^{-4}	1.71×10^{-4}	3.60	2.10	2.28
338.15	200	2.45×10^{-4}	2.39×10^{-4}	4.35	1.82	2.44
338.15	280	4.92×10^{-4}	4.87×10^{-4}	5.19	1.06	1.01

* Calculated based on our experimental data.
** Calculated based on our experimental data and literature data (Li et al., 2019), $AARD\% = \sum_{i=1}\left|\frac{y_i^{Exp.} - y_i^{Calc.}}{y_i^{Exp.}}\right| \times 100$.

not accessible for all components. Furthermore, the SAFT family EoSs have at least three fitting parameters, which must be fitted by experimental vapor pressure or density of pure component (Chapman et al., 1989; Gross and Sadowski, 2002; Gross and Sadowski, 2001).

As far as we know, no investigation is presented for the measurement of the *digitoxin* drug solubility in supercritical CO_2. The main motivation of this study is measurement of *digitoxin* drug solubility in SC—CO_2. The drug solubility measurement was performed in following range of temperature and pressure: $311 < T\,(K) < 343$ and $120 < P\,(bar) < 300$. For evaluation of experimental setup, the solubility of *ketoprofen* drug was obtained and the results were compared with the presented experimental data. After that and for investigation of the drug-CO_2phase behavior, two various groups of equations were considered, i.e. cubic/non-cubic equations of state (EoS) and semi-empirical correlations. SAFT (statistical associating fluid theory) EoS and sPC-SAFT (simplified perturbed-chain statistical associating fluid theory) EoS, SRK (Soave-Redlich-Kwong) EoS are cubic/non-cubic EoS and Kumar-Johnston (K-J), Garlapati-Madras (GM), Mendez-Santiago-Teja (MST), Bartle et al., Sung-Shim and Chrastil models are six popular semi-empirical correlations.

2. Material and method

2.1. Material

Digitoxin is a cardiac glycoside applied for the treatment of heart arrhythmia and heart failure. After characterization, *Digitoxin* shows an amorphous phase with some crystallinity (the X-Ray diffraction analysis (XRD) pattern is presented in the Supplementary file). The solubility of *digitoxin* drug in water is very low and is known as poor water-soluble (He et al., 2021; Haux, 1999; Wang et al., 2011; Dai et al., 2020; Cai et al., 2014; https://webbook.nist). More information of all substances is tabulated in Table 1 and the structure of *digitoxin* is illustrated in Fig. 1. No additional treatment was carried out for the substances before use.

2.2. Supercritical CO_2 setup and procedure

We utilized a straightforward method to measure the *digitoxin* drug solubility in supercritical CO_2, as previously described in research researches (Bagheri et al., 2022; Notej et al., 2023). The schematic of the laboratory setup is given in Fig. 2. All the piping, connections and equipment were constructed from stainless steel 316.

With respect to Fig. 2, the laboratory setup is composed of a (1) carbon dioxide tank, (2) needle valve, (3) filter (pore size = 1 μm), (4) refrigerator unit, (5) high-pressure reciprocating pump (an air-driven liquid pump, type-M64, Shineeast Co., China), (6) compressor, (7) oven, (8) heating coil, (9) equilibrium column (200 mL), (10) syringe, (11) back pressure regulator, (12) micrometer valve, (13) collection vial, (14) UV–Vis Spectrophotometer (UNICO-4802 UV–Vis), and (15) automation. More details of supercritical setup performance were given else ever (Wang et al., 2011; Dai et al., 2020). First, CO_2 enters the refrigerator unit once it has passed through a filter. The purpose of this unit is to completely liquefy CO_2 by reducing the temperature from room temperature to approximately −25 °C. CO_2, in the liquid state, at the pressure of around 60 bar, which is the pressure in the carbon dioxide

Table 3
The information of all used thermodynamic equations for solubility modeling of *digitoxin* drug.

Semi-empirical correlations Correlation (AARD %)	a	b	c	d
Chrastil (7.89): $\ln S = a\ln(\rho_{SC-CO_2}) + b + \frac{c}{T}$	4.5074	−14.6398	−5645.1730	
KJ (6.25): $\ln y = a + b \times \rho_{SC-CO_2} + \frac{c}{T}$	−3.9691	0.0056	−4023.3374	
MST (7.17): $\ln\left(\frac{yP}{P_{Ref.}}\right) = \frac{a}{T} + \frac{b\rho_{SC-CO_2}}{T} + c$	−7903.6640	3.2371	9.8558	
GM (11.04): $\ln y = a + \frac{b}{T} + c\ln(\rho_{SC-CO_2} \times T)$	−11.1004	−1732.9526	4.6427	
Bartle et al., (8.06): $\ln\left(\frac{yP}{P_{Ref.}}\right) = a + b(\rho_{SC-CO_2} - \rho_{Ref.}) + \frac{c}{T}$	16.9229	0.0099	−7814.0024	
Sung-Shim (12.14): $\ln y = \left(a + \frac{b}{T}\right) \times \ln(\rho_{SC-CO_2}) + \frac{c}{T} + d$	5.3671	−344.1417	414.7783	−42.0863
sPC-SAFT EoS				
T (K)		**AARD%**		
311		9.05		
323		8.78		
333		6.01		
343		11.97		
Total AARD%		**8.96**		
SAFT EoS				
T (K)		**AARD%**		
311		11.23		
323		10.06		
333		8.24		
343		14.70		
Total AARD%		**11.05**		
SRK EoS				
T (K)		**AARD%**		
311		12.65		
323		14.82		
333		16.31		
343		19.98		
Total AARD%		**15.94**		

reservoir, was pumped to the desired pressure by using the high-pressure pump. By using the transmitter and pressure gauge, measurements were done at an accuracy of ±1 bar. To maintain a stable temperature during the experiment, the equilibrium column was placed in a precise oven with a temperature accuracy of ±0.1 K. Each experimental run involved placing 2 g of *digitoxin* in the equilibrium column. To prevent any un-dissolved *digitoxin* drug from being physically mixed in, stainless steel sintered filters (1 μm) were installed on both ends of the high-pressure equilibrium column. To achieve the desired pressure, CO_2 was added to the equilibrium column. Afterward, the system was allowed to reach equilibrium for a period of 4 h. The 3-way valve was applied to inject the saturated SC—CO_2 into a sampling loop. After that, the sampling loop was depressurized into a certain amount of MeOH. In this part and for controlling the flow, the micrometer valve was applied. To finish and for washing the loop, 1 ml of methanol was introduced into the loop using a syringe and the final solution volume in the collection vial amounted to 5 mL. The method was conducted three times for each data.

Table 4
The *digitoxin* drug solubility in supercritical CO_2 at various conditions.

P (bar)	(Solubility) × 10^5	ρ_{CO2} (kg/m^3) (https)	S (kg/m^3)	SD × 10^6	RSD
$T = 311$ K					
120	0.32	739.09	0.0411	0.31	9.68
150	0.45	795.64	0.0622	0.32	7.12
180	0.56	832.33	0.0810	0.34	6.07
210	0.66	860.14	0.0986	0.36	5.46
240	0.71	882.77	0.1089	0.41	5.77
270	0.78	902.02	0.1222	0.52	6.67
300	0.87	918.84	0.1389	0.54	6.21
$T = 323$ K					
120	0.25	583.48	0.0253	0.26	10.40
150	0.36	699.76	0.0437	0.36	10.00
180	0.51	757.77	0.0671	0.34	6.67
210	0.60	796.83	0.0831	0.37	6.16
240	0.76	826.64	0.1092	0.51	6.71
270	0.88	850.91	0.1301	0.53	6.02
300	1.01	871.51	0.1529	0.61	6.04
$T = 333$ K					
120	0.16	439.25	0.0122	0.21	12.50
150	0.28	604.05	0.0293	0.23	8.21
180	0.42	687.51	0.0502	0.40	9.52
210	0.56	739.35	0.0719	0.34	6.18
240	0.81	776.81	0.1093	0.52	6.41
270	0.97	806.26	0.1359	0.62	6.43
300	1.08	830.60	0.1560	0.95	8.84
$T = 343$ K					
120	0.095	349.08	0.0057	0.62	6.58
150	0.23	508.18	0.0203	0.20	8.69
180	0.38	612.92	0.0404	0.26	6.96
210	0.57	678.71	0.0672	0.34	6.08
240	0.85	724.84	0.1071	0.46	5.39
270	1.03	760.11	0.1360	0.98	9.57
300	1.12	788.65	0.1535	0.96	8.52

The solubility of the *digitoxin* drug was obtained using absorbency measurements at a maximum wavelength ($\lambda_{max} = 228$ nm) with UV–Vis spectrophotometer with 1-cm pass length quartz cells. The calibration curve was obtained (R^2 set to 0.995) and was used to specify the concentration of *digitoxin* in the collection vial.

The drug solubility measurement device was validated using assessing the solubility of the *ketoprofen* drug under various conditions. The results obtained were then compared to those found in the literature (Sabegh et al., 2012) (see Table 2).

The reliability of the used approach is demonstrated by using the relative standard deviation and relative standard deviation parameters. Furthermore, we assessed the performance of SC—CO_2 apparatus by measured the solubility of *paracetamol* (Bagheri et al., 2022), *salicylic acid* (Bagheri et al., 2022) and *mefenamic acid* (Bagheri et al., 2022), *phenytoin* (Notej et al., 2023), *raloxifene* (Notej et al., 2023) and aspirin (Notej et al., 2023).

3. SC—CO_2/*Digitoxin* phase equilibria

In this study, two various groups of models were studied for modeling the solubility of *digitoxin* drug in supercritical carbon dioxide, including six semi-empirical models (KJ (Kumar and Johnston, 1988), MST (Méndez-Santiago and Teja, 1999), GM (Garlapati and Madras, 2010), Bartle et al., (Bartle et al., 1991), Sung-Shim (Sung and Shim, 1999) and Chrastil (Chrastil, 1982) models) and cubic (SRK EoS) and non-CEoSs (SAFT, sPC-SAFT EoS) (Wang et al., 2011; Cai et al., 2014, https).

The *digitoxin* solubility in supercritical CO_2 is measured according to

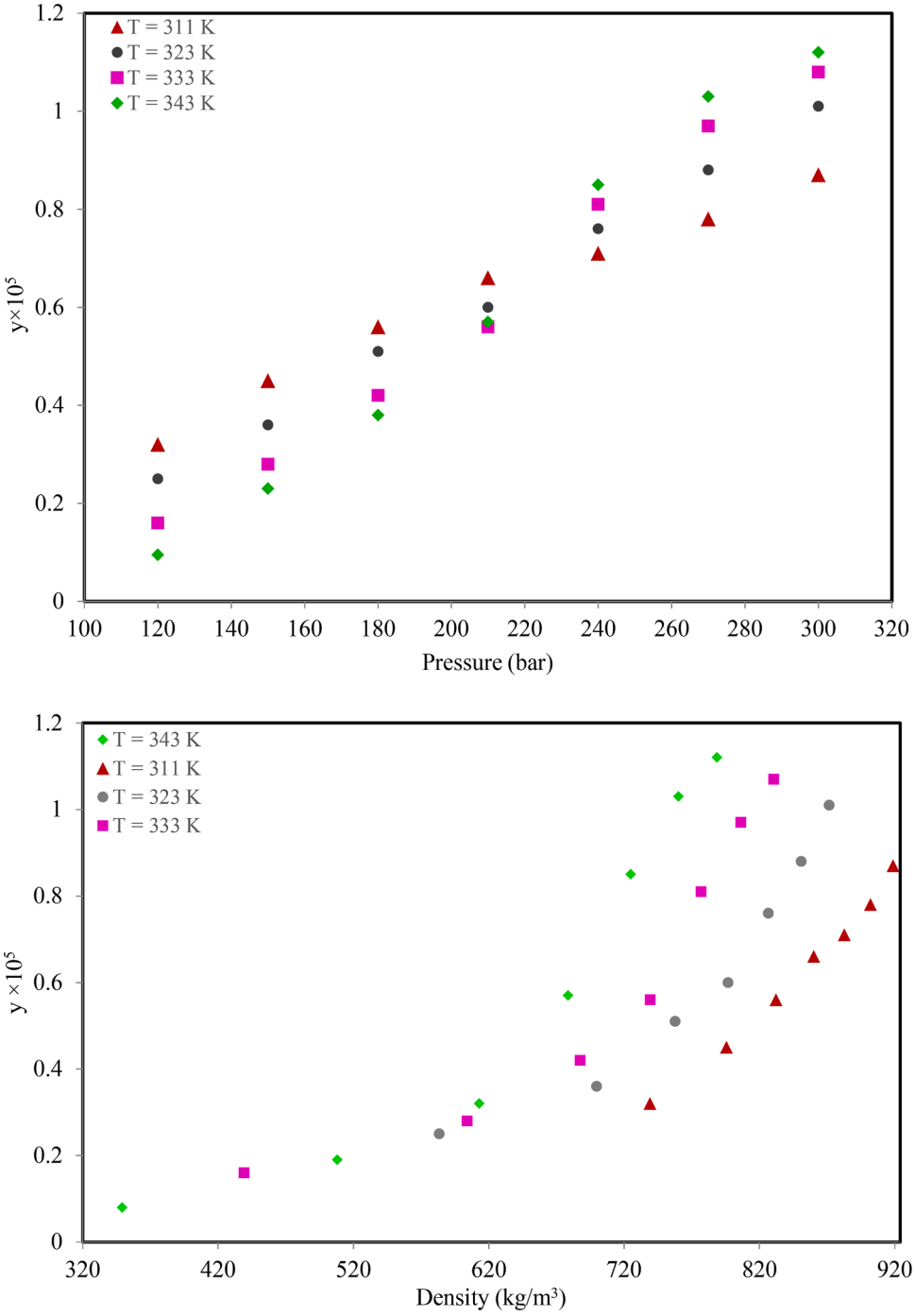

Fig. 3. The behavior of measured *digitoxin* solubility and the operational pressure/density.

the following (Bagheri et al., 2018):

$$\widehat{f}_1^{Sup.} = f_1^{drug} \tag{1}$$

where

$$\widehat{f}_1^{Sup.} = y_1 P \, \widehat{\varphi}_1^{Sup.} \tag{2}$$

$$f_1^{drug} = \varphi_1^{sat.} P_1^{sat.} exp\left[\int_{P_1^{sat.}}^{P} \left(\frac{v_1^{drug}}{RT}\right) dP\right] = \varphi_1^{sat.} P_1^{sat.} exp\left[\frac{v_1^{drug}\left(P - P_1^{sat.}\right)}{RT}\right] \tag{3}$$

Thus, *digitoxin* drug solubility is mathematically expressed by (Bagheri et al., 2022; Notej et al., 2023):

$$y_1 = \frac{\varphi_1^{sat.} P_1^{sat.} exp\left[\frac{v_1^{drug}\left(P - P_1^{sat.}\right)}{RT}\right]}{P \, \widehat{\varphi}_1^{Sup.}} \tag{4}$$

To calculate the fugacity coefficient of *digitoxin* drug ($\widehat{\varphi}_1^{Sup.}$), SRK, SAFT sPC-SAFT EoSs were used. More details of all EoSs are given in the literature [(Sodeifian et al., 2023; Bagheri et al., 2018; Chapman et al., 1989; Gross and Sadowski, 2002; Gross and Sadowski, 2001) (Bagheri et al., 2023)] and Appendix A. Moreover, the details of used semi-empirical correlations are given in Table 3.

Table 5
The SAFT and sPC-SAFT EoSs parameters, *digitoxin* and CO_2.

Substance	m	σ (Å)	ε/k_B (K)	ε^{AB}/k_B (K)	κ^{AB}	Ref.
sPC-SAFT EoS						
Digitoxin	3.1941	4.3509	401.0665	5972.2678	0.0867	This study
CO_2	2.8246	2.8147	160.1094			42
SAFT EoS						
Digitoxin	2.0632	3.1649	573.9856	4792.6458	0.0569	This study
CO_2	3.4207	15.1792	220.0871			This study

4. Results and discussion

4.1. Experimental results

The solubility of *digitoxin* drug in supercritical carbon dioxide was measured at different operational temperatures (311–343 K) and pressures (120–300 bar), based on the mentioned procedure in Section 2.2. The solubility of the *digitoxin* drug is measured based on the following correlation (Bagheri et al., 2022):

$$y_{drug} = \frac{C_{drug} \times V_C \times M_{w,CO_2}}{C_{drug} \times V_C \times M_{w,CO_2} + V_S \times \rho \times M_{w,drug}} \quad (5)$$

In the above relationships, V_S is the vial collection volume and V_C is the collection sampling loop volume, and other parameters are specified. Also, the equilibrium solubility parameter was calculated based on the following correlation (Sodeifian et al., 2023):

$$S = \frac{\rho \times M_{w,drug} \times y_{drug}}{M_{w,CO_2} \times (1 - y_{drug})} \quad (6)$$

The resultants based on the mole fraction and equilibrium solubility parameter of the *digitoxin* drug are tabulated in Table 4 and depicted in Fig. 3.

Clearly visible, a direct connection between the *digitoxin* solubility and the operational pressure is detected. This means that, when the operational temperature remains constant, an increase in operational pressure results in an increase in *digitoxin* solubility (see Fig. 3). As a matter of fact, because of reducing the distance of intermolecular among the CO_2 molecules and the increase of CO_2 density, which results to increase the intermolecular interactions of *digitoxin*-CO_2 and increasing the solvation power of supercritical CO_2. Similar results were reported in the literature (Sabegh et al., 2012; Sodeifian et al., 2023; Bagheri et al., 2022; Notej et al., 2023). In reverse, the investigation of the effect of operational temperature on the solubility of *digitoxin* is not straightforward. Referring to Fig. 3, at P (bar) < 220, the solubility of *digitoxin*, at higher operational temperatures, is less in comparison with lower operational temperatures. Nonetheless at operational pressures more than 220 bar, P (bar) > 220, increasing in the operational temperature leads to increasing in the *digitoxin* solubility. Therefore, P (bar) $\cong 220$ is a crossover point of the *digitoxin*-supercritical CO_2 binary system. At the crossover point, the density of SCF is the dominant parameter for the calculation of the *digitoxin* solubility. As operational pressures increase, the sublimation pressure of *digitoxin* also increases with increasing temperatures, resulting in an observed increase in *digitoxin* solubility. This behavior has been previously reported by other researchers (Sodeifian et al., 2023; Bagheri et al., 2022; Notej et al., 2023; Sodeifian et al., 2018).

The solubility of a compound in supercritical CO_2 is mostly determined by the amount of amorphous material present. This is because the increased disorder and free space in the amorphous structure enable better penetration of CO_2 and diffusion of the solute. Hence, the existence of a somewhat crystalline structure inside the mostly amorphous matrix would have minimal effect on the measurements of solubility, since the dissolution process in supercritical CO_2 is mostly aided by the amorphous regions.

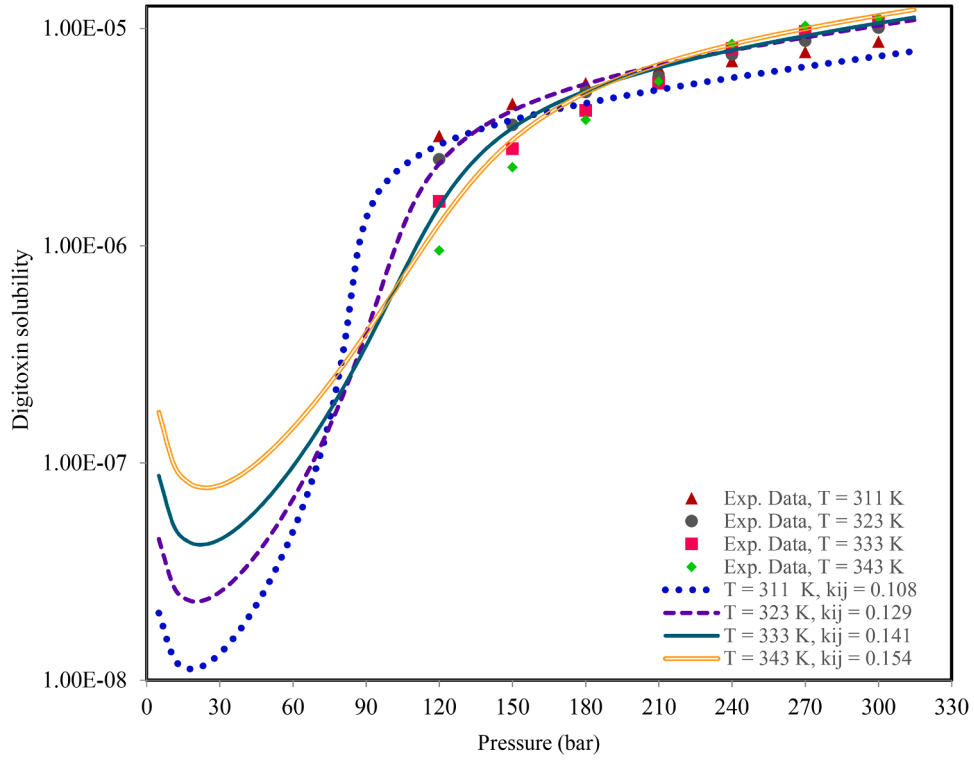

Fig. 4. The results of the sPC-SAFT EoS: *digitoxin*-supercritical CO_2 system.

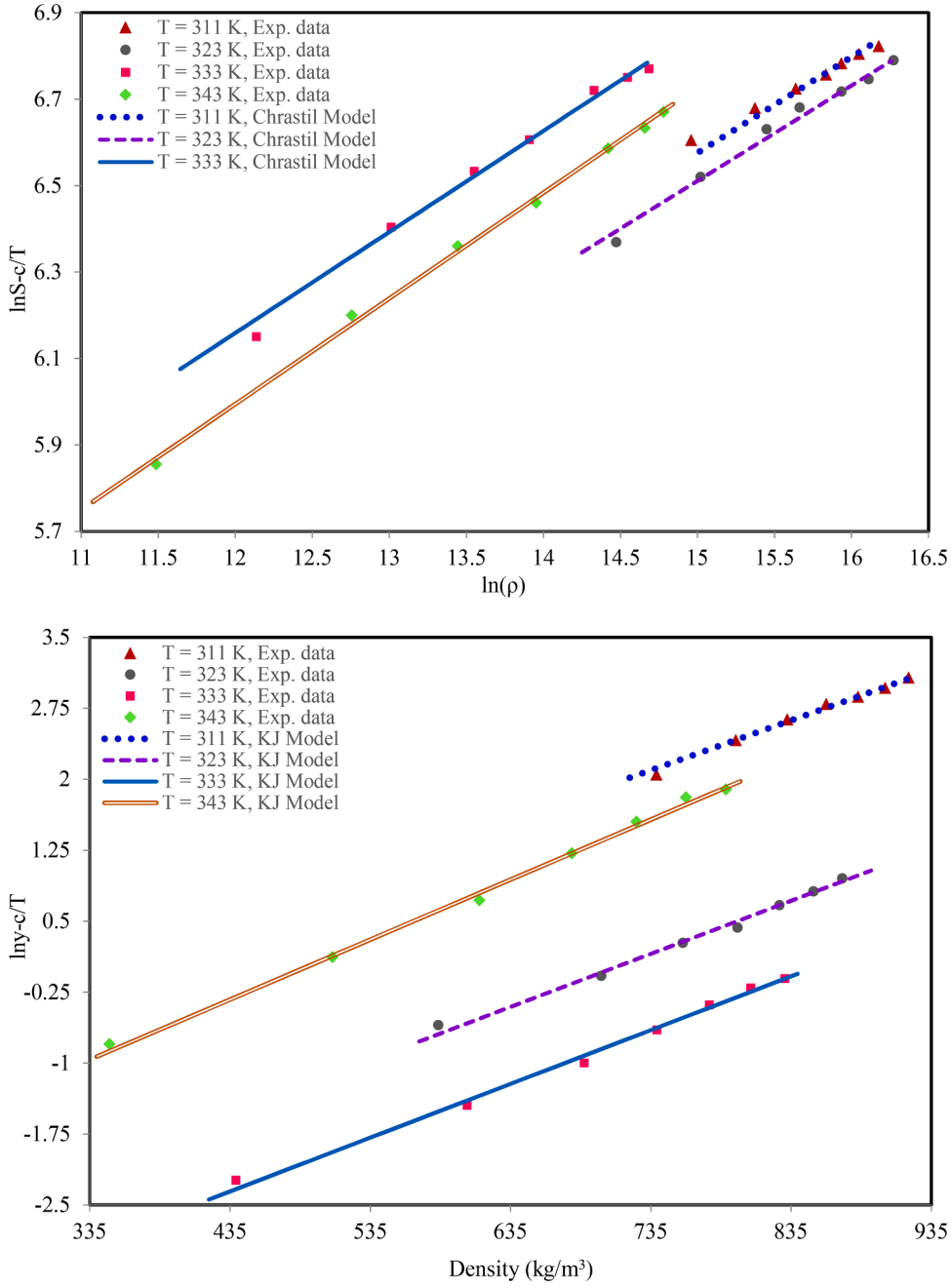

Fig. 5. Correlated *digitoxin* solubility data using semi-empirical models.

4.2. Theoretical study of digitoxin solubility

4.2.1. Cubic/Non-Cubic EoSs

As mentioned, the resultants of experimental data of *digitoxin* were modeled by semi-empirical correlations and cubic/non-CEoSs. For the first step, the parameters of SAFT and sPC-SAFT EoSs of carbon dioxide and *digitoxin* must be calculated. The SAFT and sPC-SAFT EoSs contains five parameters in order: three parameters for non-associating components (m (segment number), ε/κ (interaction energy) and σ (hard core segment radius)) and two parameters for associating components (κ^{AB} (association co-volume) and ε^{AB} (association energy)). The SAFT and sPC-SAFT EoSs use similar association terms. Similar to a procedure that was presented in the reference (Sodeifian et al., 2018), the parameters of *digitoxin* were obtained using curve-fitting with experimental solubility data, such that $k_{ij} = 0$ (BIP, binary interaction parameter). The obtained parameters are given in Table 5.

The accuracy of the mentioned equations to fit the experimental data is evaluated by using the AARD% value. It was computed as follows:

$$AARD\%\ (average\ absolute\ relative\ deviation) = \frac{1}{N}\sum_{i=1}\left|\frac{y_i^{Exp.} - y_i^{Calc.}}{y_i^{Exp.}}\right| \times 100 \quad (7)$$

where $y_i^{Exp.}$, $y_i^{Calc.}$ and N are the experimental *digitoxin* solubility value, the resultant solubility value based on the desired model, and the number of experimental data, respectively.

The SAFT EoS only considers the shape of molecules in the repulsive part of the equation, while sPC-SAFT EoSs also accounts for the chain

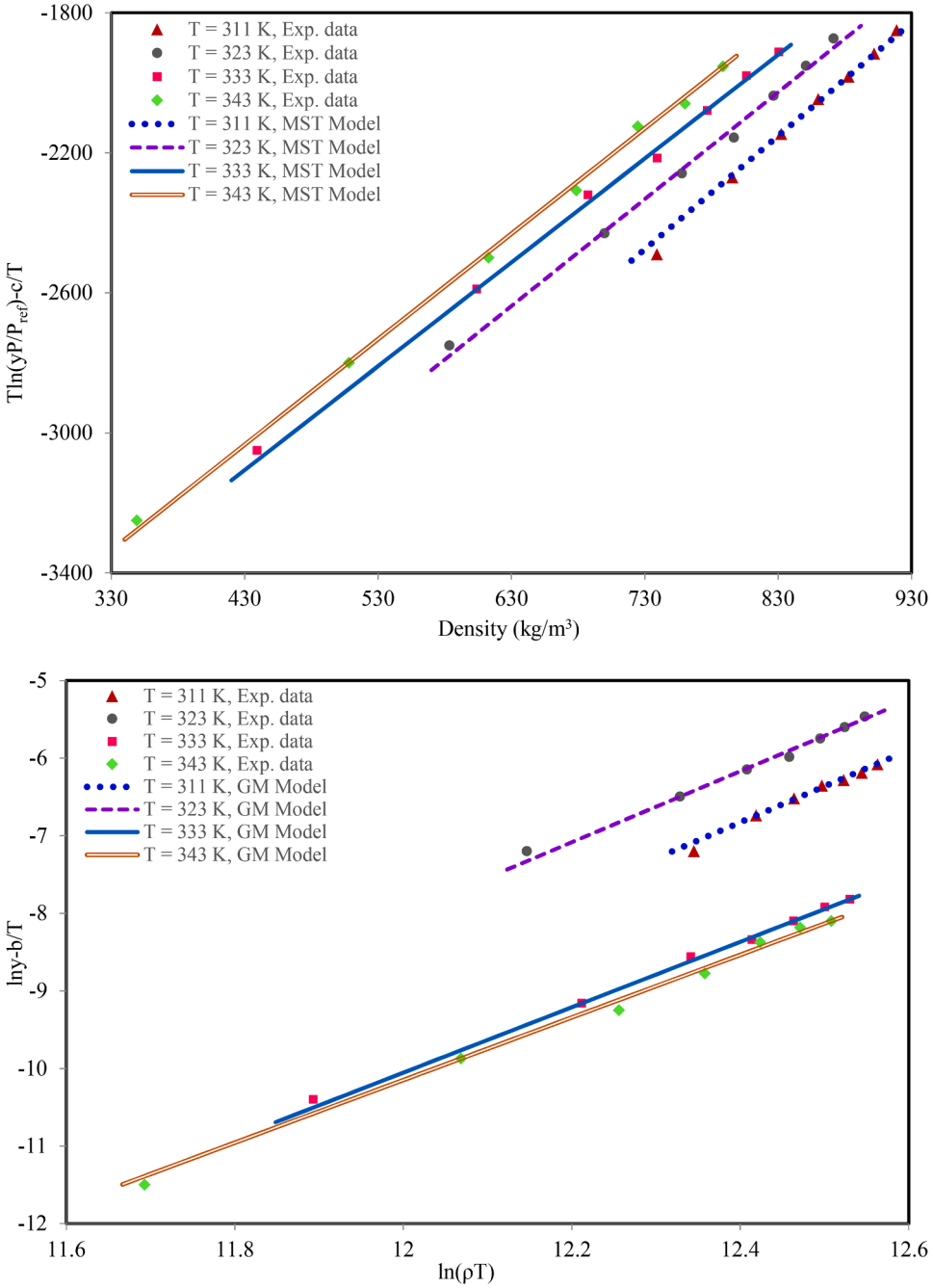

Fig. 5. (*continued*).

length in the attractive interactions. The PC-SAFT model is suitable for pure components and mixtures of solvents and gases. In the case of SRK EoS as CEoS, these types of CEoSs consider only repulsive and attractive forces and at high pressures so, SRK EoS shows poor capability for modeling drug solubility. The sPC-SAFT EoS performs better than other EoSs. The results of the *digitoxin* solubility modeling at temperatures of 311, 323, 333, and 343 K by the sPC-SAFT equation of state in the considered operational pressure range, are illustrated in Fig. 4. The sPC-SAFT EoS used a BIP (k_{ij}).

Applying the BIP results in significant improvements and decreases the average absolute relative deviation. The values of binary interaction were positive. Referring to experimental solubility values, at constant operational temperature and by increasing the operational pressure, higher solubility values of the *digitoxin* in SC—CO_2 will be obtained. The sPC-SAFT EoS follows this trend with acceptable accuracy and the resultants have less relative deviation. The sPC-SAFT equation of state can foresee the *digitoxin* solubility with more accuracy, particularly at high pressures, and better agreement between the *digitoxin* drug solubility experimental data and modeling resultants of mole fractions is observed. It is important to note that, at high operational pressure, the interactions between molecules are crucial, and it is necessary to use an equation of state that can accurately depict these interactions. Some researchers have offered the SAFT family as an equation with a powerful thermodynamic base for modeling solid solubility in supercritical fluids (Chapman et al., 1989; Gross and Sadowski, 2002; Gross and Sadowski, 2001; Anvari and Pazuki, 2014). Moreover, Bagheri et al. (Bagheri et al., 2022) and Sodeifian et al. (2018) applied the SAFT family equations of state to model the solubility of two various drugs in supercritical carbon dioxide. They used sPC-SAFT EoS for the paracetamol/SC—CO_2 binary system and PCP-SAFT EoS for the *Ketotifen* fumarate/supercritical

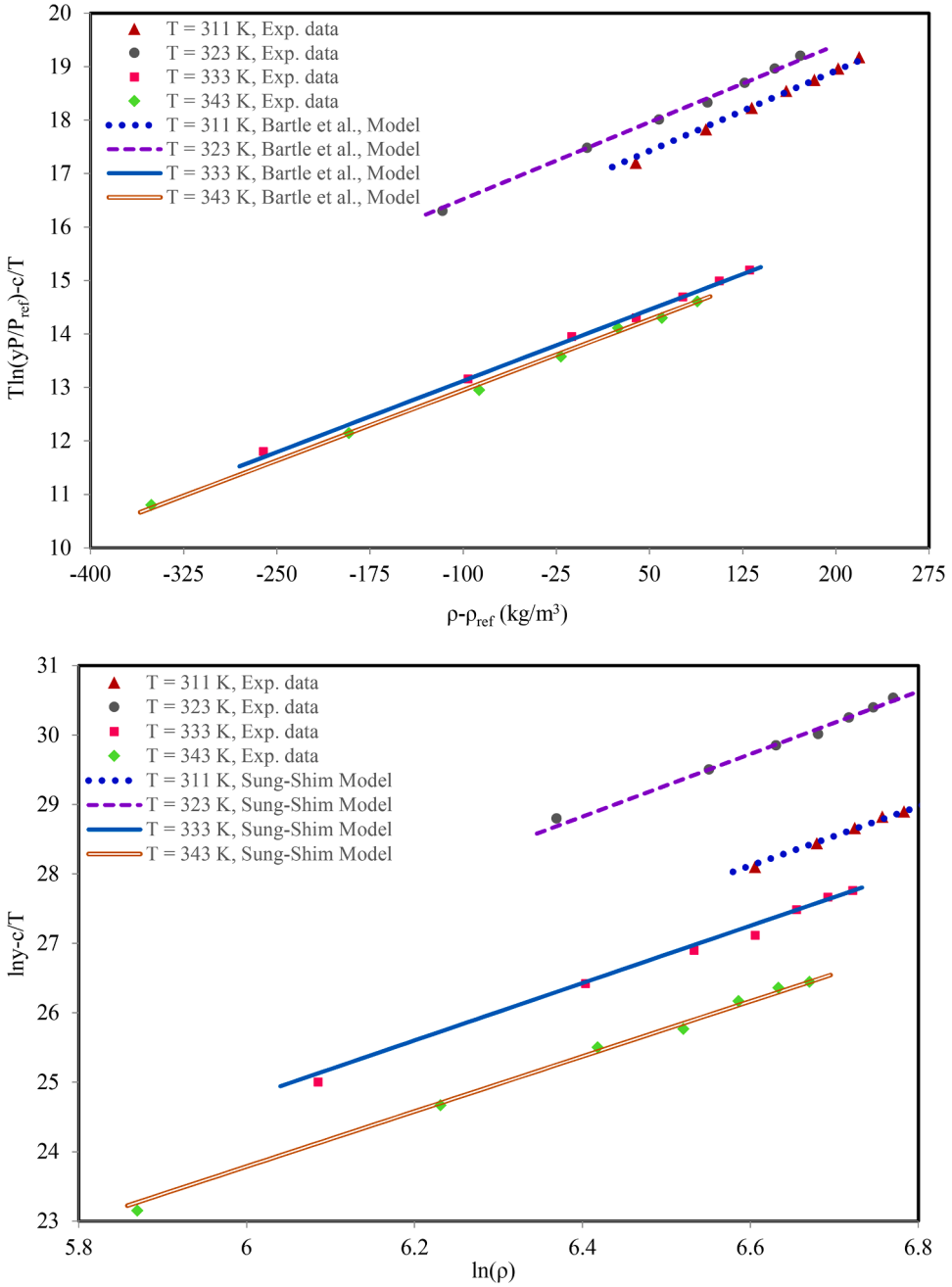

Fig. 5. (*continued*).

carbon dioxide binary system. The resultants showed that, the SAFT family EoSs could predict solubility of drugs with good agreement. Besides, the AARD values of the SRK, SAFT, sPC-SAFT equations of state are given in Table 3.

4.2.2. *Semi-Empirical correlations*

Some semi-empirical correlations such as Chrastil, Kumar-Johnston, Sung-Shim, Bartle et al., Mendez-Santiago-Teja and Garlapati and Madras models were applied for correlating *digitoxin* drug solubility in SC—CO_2 at different operational pressures and temperatures. For evaluation of the capabilities of six semi-empirical correlations, the AARD parameter was applied as statistical criteria for comparison between the obtained resultants and drug solubility data (see Table 3). The modeling resultants are given in Fig. 5.

The semi-empirical correlation parameters were obtained by the GA (genetic algorithm) tool (Bagheri et al., 2021; Bagheri et al., 2021; Bagheri and Ghader, 2017; Sheikhi-Kouhsar et al., 2015; Mokhtari et al., 2022; Bagheri and Mohebbi, 2017) and the results are tabulated in Table 3. As is evident, the AARD values are in the range of 6.25 to 12.14. Among all used models, KJ, and MST models with AARD% = 6.25, and AARD% = 7.17, respectively indicate more association with drug solubility data. These semi-correlations are three-parameter correlations. Furthermore, the Sung-Shim model, as four-parameter model, with AARD% = 12.14 shows acceptable behavior referring to experimental solubility data. The examined correlations are accurate and can be used to make predictions. Based on the values of AARD% for each of the investigated semi-empirical correlations, it is obvious that all of them applied in this communication can accurately model the *digitoxin* solubility in SC—CO_2. The used semi-empirical correlations can be applied to calculate the *digitoxin* solubility within the specified pressure and temperature ranges, according to the obtained adjustable parameters. These correlations are simple and accurate, making them good for

modeling drug solubility data.

The ability of computing ΔH_{tot} and ΔH_{vap} of the *digitoxin*-supercritical carbon dioxide binary mixture is one of the advantages of the semi-empirical correlations. The mentioned enthalpies can be calculated based on *c* parameter of KJ, Chrastil and Bartle et al. models through the following relationships:

$$\Delta H_{tot.}(total\ enthalpy) = -c_{KJ} \times R = 33.45\ kJ.mol^{-1} \quad (8)$$

$$\Delta H_{tot.}(total\ enthalpy) = -c_{Chrastil} \times R = 46.93\ kJ.mol^{-1} \quad (9)$$

$$\Delta H_{vap.}(vaporization\ enthalpy) = -c_{Bartle\ et\ al.} \times R = 64.97\ kJ.mol^{-1} \quad (10)$$

According to the Hess's law, ΔH_{sol} of the *digitoxin*-supercritical carbon dioxide binary mixture is following:

$$\Delta H_{sol.}(solvation\ enthalpy) = \Delta H_{tot.KJ} - \Delta H_{vap.Bartle\ et\ al.} = -31.52\ kJ.mol^{-1} \quad (11)$$

$$\Delta H_{sol.}(solvation\ enthalpy) = \Delta H_{tot.Chrastil} - \Delta H_{vap.Bartle\ et\ al.} = -18.04\ kJ.mol^{-1} \quad (12)$$

5. Conclusions

Supercritical CO_2 refers to carbon dioxide that is above its critical pressure and temperature. SC—CO_2 has unique properties that make it useful in various industries. It has improved solvation properties and mass transfer. These properties make it suitable for tasks like increasing water insoluble drugs. In this communication, the *digitoxin* solubility in SC—CO_2 was measured at 120–300 bar and 311–343 K in the range of 0.095×10^{-5} to 1.12×10^{-5}. Changing pressure and temperature can impact the solubility of *digitoxin* in supercritical carbon dioxide. The measurements showed that pressure and temperature affect the solubility of *digitoxin* in supercritical CO_2. At higher pressures, the solubility increases because SC—CO_2 has a higher solvating power due to its higher density. Below a pressure of 220 bar, temperature has a reverse effect on solubility because it reduces density, but above this pressure, increasing temperature increases solubility due to solid sublimation pressure compensating for density reduction. This leads to higher solubility of *digitoxin* in SC—CO_2. The measured experimental data were modeled through SAFT, sPC-SAFT, SRK EoSs and six semi-empirical models (Chrastil, Kumar-Johnston, Garlapati and Madras, Mendez-Santiago-Teja, Bartle et al., and Sung-Shim). The cubic/non-cubic EoSs and density-based models were adjusted to fit experimental solubility data and assessed based on the AARD values. The results showed that the sPC-SAFT EoS and KJ correlations had good agreement with the experimental data for *digitoxin* solubility, with an AARD% of 8.96 and 6.25, respectively. Finally, the total, solvation and vaporization enthalpies of the *digitoxin*-supercritical CO_2 binary mixture were calculated using Bartle et al., Chrastil, and Kumar-Johnston correlations. The use of SC—CO_2 for extracting useful substances and preparing drugs needs more research on a larger scale. It is also important to analyze the cost and environmental impact of this process. This information will help determine if using SC—CO_2 in drug solubility for micronation of valuable drug is a good idea. Indeed, the research found that *digitoxin* can be used in new technologies to make its particles smaller and change their shape. This could make it easier to use in medical treatments. To micro/nanozation of low of non-water-soluble drugs, such as *digitoxin*, based on SCF processes, the drug solubility experimental data is the first and main step. So, the experimental solubility results that are obtained in this investigation, are valuable to reduce particle size of *digitoxin* drug via RESS (rapid expansion of supercritical solutions) and SAS (supercritical anti-solvent) processes.

CRediT authorship contribution statement

Mohammadreza Sheikhi-Kouhsar: Writing – review & editing, Writing – original draft, Visualization, Validation, Supervision, Software, Resources, Methodology, Investigation, Formal analysis, Data curation. **Hamidreza Bagheri:** Writing – review & editing, Writing – original draft, Visualization, Supervision, Software, Project administration, Methodology, Investigation, Formal analysis, Data curation, Conceptualization. **Fahad Alsaikhan:** Writing – review & editing, Visualization, Validation, Supervision, Software, Resources, Methodology, Investigation, Data curation. **Ahmed Khalid Aldhalmi:** Writing – review & editing, Validation, Software, Resources, Investigation, Formal analysis, Conceptualization. **Hanan Hassan Ahmed:** Writing – review & editing, Visualization, Supervision, Software, Resources, Project administration, Investigation, Formal analysis, Data curation, Conceptualization.

Data availability

Data will be made available on request.

Acknowledgements

This study is supported via funding from Prince Sattam Bin Abdulaziz University project number (PSAU/2023/R/1444).

Supplementary materials

Supplementary material associated with this article can be found, in the online version, at doi:10.1016/j.ejps.2024.106731.

Appendix A

The simplified perturbed chain statistical associating fluid theory equation of state is expressed as follows (Sodeifian et al., 2024; Chapman et al., 1989; Gross and Sadowski, 2002):

$$\frac{A^{res}}{NkT} = \frac{A^{hs}}{NkT} + \frac{A^{disp}}{NkT} + \frac{A^{assoc}}{NkT} \quad (A.1)$$

$$\frac{A^{hc}}{NkT} = \overline{m}\frac{A^{hs}}{NkT} - \sum_i y_i(m_i - 1)\ln g_{ii}^{hs}(\sigma_{ii}) \quad (A.2)$$

$$\overline{m} = \sum_i y_i m_i \quad (A.3)$$

$$\frac{A^{hs}}{NkT} = \frac{4\eta - 3\eta^2}{(1-\eta)^2} \quad (A.4)$$

$$\zeta_n = \frac{\pi}{6}\rho\sum_i y_i m_i d_i^n \tag{A.5}$$

$$\rho = \frac{6}{\pi}\frac{\eta}{\sum_i y_i m_i d_i^3} \tag{A.6}$$

$$g^{hs} = \frac{2-\eta}{2(1-\eta)^3} \tag{A.7}$$

$$d_i = \sigma_i\left[1-0.12exp\left(\frac{-3\varepsilon_i}{kT}\right)\right] \tag{A.8}$$

$$\frac{A^{disp}}{NkT} = -2\pi\rho I_1(\eta,\overline{m})\overline{m^2\varepsilon\sigma^3} - \pi\rho\overline{m}C_1 I_2(\eta,\overline{m})\overline{m^2\varepsilon^2\sigma^3} \tag{A.9}$$

$$C_1 = \frac{1}{1+\overline{m}\frac{8\eta-2\eta^2}{(1-\eta)^4}+(1-\overline{m})\frac{20\eta-27\eta^2+12\eta^3-2\eta^4}{[(1-\eta)(2-\eta)]^2}} \tag{A.10}$$

$$\overline{m^2\varepsilon\sigma^3} = \sum_i\sum_j y_i y_j m_i m_j\left(\frac{\varepsilon_{ij}}{kT}\right)\sigma_{ij}^3 \tag{A.11}$$

$$\overline{m^2\varepsilon^2\sigma^3} = \sum_i\sum_j y_i y_j m_i m_j\left(\frac{\varepsilon_{ij}}{kT}\right)^2\sigma_{ij}^3 \tag{A.12}$$

$$\sigma_{ij} = \frac{1}{2}(\sigma_i+\sigma_j) \tag{A.13}$$

$$\varepsilon_{ij} = \sqrt{\varepsilon_i\varepsilon_j}\,(1-k_{ij}) \tag{A.14}$$

$$I_1(\eta,\overline{m}) = \sum_{i=0}^{6} a_i(\overline{m})\,\eta^i \tag{A.15}$$

$$I_2(\eta,\overline{m}) = \sum_{i=0}^{6} b_i(\overline{m})\,\eta^i \tag{A.16}$$

$$a_i(\overline{m}) = a_{0i} + a_{1i}\frac{\overline{m}-1}{\overline{m}} + a_{2i}\frac{\overline{m}-1}{\overline{m}}\frac{\overline{m}-2}{\overline{m}} \tag{A.17}$$

$$b_i(\overline{m}) = b_{0i} + b_{1i}\frac{\overline{m}-1}{\overline{m}} + b_{2i}\frac{\overline{m}-1}{\overline{m}}\frac{\overline{m}-2}{\overline{m}} \tag{A.18}$$

$$\frac{A^{assoc}}{RT} = \sum_i y_i\left[\sum_{A_i}\left(\ln X^{Ai}-0.5X^{Ai}\right)+0.5M_i\right] \tag{A.19}$$

$$X^{Ai} = \frac{1}{1+N_{Av}\sum_j\sum_{B_j}\rho y_j X^{Bj}\Delta^{A_iB_j}} \tag{A.20}$$

$$\Delta^{A_iB_j} = \sigma_{ij}^3 g^{hs} K^{A_iB_j}\left[\exp\left(\frac{\varepsilon^{A_iB_j}}{kT}\right)-1\right] \tag{A.21}$$

$$K^{A_iB_j} = \sqrt{K^{A_iB_i}\,K^{A_jB_j}} \tag{A.22}$$

$$\varepsilon^{A_iB_j} = \frac{\varepsilon^{A_iB_i}+\varepsilon^{A_jB_j}}{2} \tag{A.23}$$

Furthermore, $\widehat{\varphi}_1^{Sup.}$ according to the sPC-SAFT EoS is (Chapman et al., 1989; Gross and Sadowski, 2002; Gross and Sadowski, 2001):

$$\ln\widehat{\varphi}_i^{Supercritical} = \frac{\mu_i^{sPC-SAFT}}{kT}+\frac{\mu_i^{assoc}}{RT} \tag{A.24}$$

where

$$\frac{\mu_i^{sPC-SAFT}}{kT} = \frac{A^{hc}}{NkT}+\frac{A^{disp}}{NkT}+\left(Z^{hc}+Z^{disp}\right)+\frac{\partial}{\partial y_k}\left(\frac{A^{hc}}{NkT}+\frac{A^{disp}}{NkT}\right)|_{T,v,yi\neq k}-\sum_{j=1}^{N}\left[y_j\left(\frac{\partial}{\partial y_k}\left(\frac{A^{hc}}{NkT}+\frac{A^{disp}}{NkT}\right)|_{T,v,yi\neq j}\right)\right] \tag{A.25}$$

$$\zeta_{n,xk} = \left(\frac{\partial\zeta_n}{\partial y_k}\right)|_{T,v,yj\neq k} = \frac{\pi\rho}{6}m_k(d_k)^n \tag{A.26}$$

$$\frac{\partial}{\partial y_k}\left(\frac{A^{hc}}{NkT}\right)|_{T,\rho,yj\neq k} = m_k\frac{A^{hs}}{NkT} + \overline{m}\frac{\partial}{\partial y_k}\left(\frac{A^{hs}}{NkT}\right)|_{T,\rho,yj\neq k} - \sum_i y_i(m_i-1)\left(g_{ii}^{hs}\right)^{-1}\left(\frac{\partial g_{ii}^{hs}}{\partial y_k}\right)|_{T,\rho,yj\neq k} \tag{A.27}$$

$$\frac{\partial}{\partial y_k}\left(\frac{A^{hs}}{NkT}\right)|_{T,\rho,yj\neq k} = \frac{\zeta_{0,yk}}{\zeta_0}\frac{A^{hs}}{NkT} + \frac{1}{\zeta_0}\left[\frac{3(\zeta_{1,yk}\zeta_2+\zeta_1\zeta_{2,yk})}{1-\zeta_3} + \frac{3\zeta_1\zeta_2\zeta_{3,yk}}{(1-\zeta_3)^2} + \frac{3\zeta_2^2\zeta_{2,yk}}{\zeta_3(1-\zeta_3)^2} + \frac{\zeta_2^3\zeta_{3,yk}(3\zeta_3-1)}{\zeta_3^2(1-\zeta_3)^3} + \left(\frac{3\zeta_2^2\zeta_{2,yk}\zeta_3-2\zeta_2^3\zeta_{3,yk}}{\zeta_3^3}-\zeta_{0,yk}\right)\ln(1-\zeta_3) + \left(\zeta_0-\frac{\zeta_2^3}{\zeta_3^2}\right)\frac{\zeta_{3,yk}}{1-\zeta_3}\right]. \tag{A.28}$$

$$\frac{\partial}{\partial y_k}\left(\frac{A^{disp}}{NkT}\right)|_{T,\rho,yj\neq k} = -2\pi\rho\left[I_{1,yk}\overline{m^2\varepsilon\sigma^3} + I_1\left(\overline{m^2\varepsilon\sigma^3}\right)_{yk}\right] - \pi\rho\left\{\left[m_kC_1I_2 + \overline{m}C_{1,yk}I_2 + \overline{m}C_1I_{2,yk}\right]\overline{m^2\varepsilon^2\sigma^3} + \overline{m}C_1I_2\left(\overline{m^2\varepsilon^2\sigma^3}\right)_{yk}\right\} \tag{A.30}$$

$$\left(\overline{m^2\varepsilon\sigma^3}\right)_{yk} = 2\,m_k\sum_j y_jm_j\left(\frac{\varepsilon_{kj}}{kT}\right)\sigma_{kj}^3 \tag{A.31}$$

$$\left(\overline{m^2\varepsilon^2\sigma^3}\right)_{yk} = 2\,m_k\sum_j y_jm_j\left(\frac{\varepsilon_{kj}}{kT}\right)^2\sigma_{kj}^3 \tag{A.32}$$

$$C_{1,yk} = C_2\,\zeta_{3,yk} - C_1^2\left\{m_k\frac{8\eta-2\eta^2}{(1-\eta)^4} - m_k\frac{20\eta-27\eta^2+12\eta^3-2\eta^4}{[(1-\eta)(2-\eta)]^2}\right\} \tag{A.33}$$

$$I_{1,yk} = \sum_{j=0}^{6}\left[a_i(\overline{m})i\zeta_{3,yk}\eta^{i-1} + a_{i,yk}\eta^i\right] \tag{A.34}$$

$$I_{2,yk} = \sum_{j=0}^{6}\left[b_i(\overline{m})i\zeta_{3,yk}\eta^{i-1} + b_{i,yk}\eta^i\right] \tag{A.35}$$

$$a_{i,yk} = \frac{m_k}{\overline{m}^2}a_{1i} + \frac{m_k}{\overline{m}^2}\left(3-\frac{4}{\overline{m}}\right)a_{2i} \tag{A.36}$$

$$b_{i,yk} = \frac{m_k}{\overline{m}^2}b_{1i} + \frac{m_k}{\overline{m}^2}\left(3-\frac{4}{\overline{m}}\right)b_{2i} \tag{A.37}$$

And the chemical potential association contribution is (Chapman et al., 1989; Bagheri et al., 2022):

$$\frac{\mu_i^{assoc}}{RT} = \sum_{A_i}\left[\ln X^{A_i} - \frac{X^{A_i}}{2}\right] + 0.5M_i + \sum_j\rho_j\sum_{A_i}\left[\left(\frac{\partial X^{A_j}}{\partial\rho_i}\right)|_{T,\rho,yj\neq k}\left(\frac{1}{X^{A_j}}-0.5\right)\right] \tag{A.38}$$

where

$$\left(\frac{\partial X^{A_j}}{\partial\rho_i}\right)|_{T,\rho j\neq k} = -\left(X^{A_i}\right)^2\left[N_{Av}\sum_{B_i}X^{B_i}\Delta^{A_j\,B_i} + \sum_k\sum_{B_k}N_{Av}\rho_k\left(\Delta^{A_j\,B_k}\left(\frac{\partial X^{\,B_k}}{\partial\rho_i}\right)|_{T,\rho j\neq k} + X^{B_k}\left(\frac{\partial\Delta^{A_j\,B_k}}{\partial\rho_i}\right)|_{T,\rho j\neq k}\right)\right] \tag{A.39}$$

$$\left(\frac{\partial\Delta^{A_j\,B_k}}{\partial\rho_i}\right)|_{T,\rho j\neq k} = d_{jk}^3\left(\frac{\partial g_{jk}\left(d_{jk}\right)^{hs}}{\partial\rho_i}\right)|_{T,\rho j\neq k}\left(\exp\left(\frac{\varepsilon^{A_j\,B_k}}{kT}\right)-1\right)K^{A_j\,B_k} \tag{A.40}$$

$$\left(\frac{\partial g_{jk}\left(d_{jk}\right)^{hs}}{\partial\rho_i}\right)|_{T,\rho j\neq k} = \frac{\pi N_{Av}}{6}m_i\left\{\frac{d_{ii}^3}{(1-\zeta_3)^2} + 3\frac{d_{jj}d_{kk}}{d_{jj}+d_{kk}}\left[\frac{d_{ii}^2}{(1-\zeta_3)^2} + \frac{2d_{ii}^3\zeta_2}{(1-\zeta_3)^3}\right] + 2\left(\frac{d_{jj}d_{kk}}{d_{jj}+d_{kk}}\right)^2\left[\frac{2d_{ii}^2\zeta_2}{(1-\zeta_3)^3} + \frac{2d_{ii}^3\zeta_2^2}{(1-\zeta_3)^4}\right]\right\} \tag{A.41}$$

Furthermore, the simplified perturbed chain statistical associating fluid theory equation of state can be expressed based on compressibility factor as follows (Sodeifian et al., 2024; Bagheri et al., 2022):

$$Z = 1 + Z^{hc} + Z^{disp} + Z^{assoc} \tag{A.42}$$

$$Z^{hc} = m\,Z^{hs} - \sum_i y_i(m_i-1)\left(g_{ii}^{hs}\right)^{-1}\rho\frac{\partial g_{ii}^{hs}}{\partial\rho} \tag{A.43}$$

$$Z^{hs} = \frac{\zeta_3}{1-\zeta_3} + \frac{3\zeta_1\zeta_2}{\zeta_0(1-\zeta_3)^2} + \frac{3\zeta_2^3-\zeta_3\zeta_2^3}{\zeta_0(1-\zeta_3)^3} \tag{A.44}$$

$$\rho\frac{\partial g_{ii}^{hs}}{\partial\rho} = \frac{\zeta_3}{(1-\zeta_3)^2} + \frac{d_id_j}{d_i+d_j}\left(\frac{3\zeta_2}{(1-\zeta_3)^2} + \frac{6\zeta_2\zeta_3}{(1-\zeta_3)^3}\right) + \left(\frac{d_id_j}{d_i+d_j}\right)^2\left(\frac{4\zeta_2^2}{(1-\zeta_3)^3} + \frac{6\zeta_2^2\zeta_3}{(1-\zeta_3)^4}\right) \tag{A.45}$$

$$Z^{disp} = -2\pi\rho\frac{\partial(\eta I_1)}{\partial\eta}\overline{m^2\varepsilon\sigma^3} - \pi\rho\overline{m}\left[C_1\frac{\partial(\eta I_2)}{\partial\eta} + C_2\eta I_2\right]\overline{m^2\varepsilon^2\sigma^3} \tag{A.46}$$

$$\frac{\partial(\eta I_1)}{\partial\eta} = \sum_{j=0}^{6} a_j(\overline{m})(j+1)\eta^j \tag{A.47}$$

$$\frac{\partial(\eta I_2)}{\partial\eta} = \sum_{j=0}^{6} b_j(\overline{m})(j+1)\eta^j \tag{A.48}$$

$$C_2 = \frac{\partial C_1}{\partial\eta} \tag{A.49}$$

$$Z^{assoc} = \sum_i y_i\frac{\mu_i^{assoc}}{RT} - \frac{A^{assoc}}{NkT} \tag{A.50}$$

The statistical associating fluid theory EoS is expressed as follows (Sodeifian et al., 2024; Chapman et al., 1989):

$$\frac{A^{res}}{NkT} = \frac{A^{seg}}{NkT} + \frac{A^{chain}}{NkT} + \frac{A^{assoc}}{NkT} \tag{A.51}$$

$$\frac{A^{seg}}{NkT} = m\left(\frac{A^{hs}}{NkT} + \frac{A^{disp}}{NkT}\right) \tag{A.52}$$

$$\frac{A^{hs}}{NkT} = \frac{4\eta - 3\eta^2}{(1-\eta)^2} \tag{A.53}$$

$$\frac{A^{disp}}{NkT} = \sum_i\sum_j D_{ij}\left(\frac{u}{kT}\right)^i\left(\frac{\eta}{\eta_0}\right)^j \tag{A.54}$$

$$\eta = \eta_0 m\frac{v^0}{v} \tag{A.55}$$

$$v^0 = v^{00}\left[1 - Cexp\left(\frac{-3u^0}{kT}\right)\right]^3 \tag{A.56}$$

$$u = u^0\left(1 - \frac{e}{kT}\right) \tag{A.57}$$

$$\frac{A^{chain}}{NkT} = (1-m)\ln\left(g^{hs}(\eta)\right) \tag{A.58}$$

$$g^{hs}(\eta) = \frac{2-\eta}{2(1-\eta)^3} \tag{A.59}$$

The SRK equation of state is expressed as follows (Bagheri et al., 2018; Bagheri et al., 2023):

$$P = \frac{RT}{v-b} - \frac{a_c\alpha(T)}{v^2+bv} \tag{A.60}$$

$$a_c = 0.42747\frac{R^2T_c^2}{P_c} \tag{A.61}$$

$$b = 0.08664\frac{R\,T_c}{P_c} \tag{A.62}$$

$$\alpha(T) = \left[1 + m\left(1 - \sqrt{\frac{T}{T_c}}\right)\right]^2 \tag{A.63}$$

$$m = 0.480 + 1.574\,\omega - 0.176\,\omega^2 \tag{A.64}$$

And in compressibility factor form (Notej et al., 2023):

$$Z^3 - Z^2 + \left(A - B - B^2\right)Z - AB = 0 \tag{A.65}$$

$$A = \frac{aP}{(RT)^2} \tag{A.66}$$

$$B = \frac{bP}{RT} \tag{A.67}$$

References

Oparin, R.D., Kurskaya, M.V., Krestyaninov, M.A., Idrissi, A., Kiselev, M.G., 2020. Correlation between the conformational crossover of carbamazepine and its polymorphic transition in supercritical CO_2: on the way to polymorph control. Europ. J. Pharmac. Sci. 146, 105273. Apr 15.

Long, B., Ryan, K.M., Padrela, L., 2019. From batch to Continuous-new opportunities for supercritical CO_2 technology in pharmaceutical manufacturing. Europ. J. Pharmac. Sci. 137, 104971. Sep 1.

Sodeifian, G., Bagheri, H., Razmimanesh, F., Bargestan, M., 2024. Supercritical CO_2 utilization for solubility measurement of Tramadol hydrochloride drug: assessment of cubic and non-cubic EoSs. J. Supercrit. Fluids, 106185. Jan 9.

Soleymani, F., Halimehjani, A.Z., Asar, F.J., Thatcher, G.R., 2023. Iodocyclization of S-(homo) propargyl dithiocarbamates: regiospecific synthesis of 2-imino (iminium)-1, 3-dithiolanes/dithianes/dithiepanes. Tetrahedron. Lett. 128, 154702. Sep 19.

Bagheri, H., Hashemipour, H., Rahimpour, E., Rahimpour, M.R., 2021a. Particle size design of acetaminophen using supercritical carbon dioxide to improve drug delivery: experimental and modeling. J. Environ. Chem. Eng 9 (6), 106384. Dec 1.

Khodov, I.A., Belov, K.V., Krestyaninov, M.A., Sobornova, V.V., Dyshin, A.A., Kiselev, M. G., 2023. Does DMSO Affect the Conformational Changes of Drug Molecules in Supercritical CO_2 Media? J. Mol. Liq, 122230. Jun 8.

Wang, Y., Zhai, W., Li, J., Liu, H., Li, C., Li, J., 2023. Friction behavior of biodegradable electrospun polyester nanofibrous membranes. Tribol. Int 188, 108891. Oct 1.

Bagheri, H., Ghader, S., Hatami, N., 2019a. Solubility of ibuprofen in conventional solvents and supercritical CO_2: evaluation of ideal and non-ideal models. Chem. Chem. Technol.,. 1. (13),. 2019 (1). Feb 281-0.

Asar, F.J., Soleymani, F., Hooshmand, S.E., Halimehjani, A.Z., 2020. Direct synthesis of piperazines containing dithiocarbamate derivatives via DABCO bond cleavage. Tetrahedron. Lett. 61 (49), 152610. Dec 3.

Karn, P.R., Cho, W., Park, H.J., Park, J.S., Hwang, S.J., 2013. Characterization and stability studies of a novel liposomal cyclosporin A prepared using the supercritical fluid method: comparison with the modified conventional Bangham method. Int. J. Nanomedicine 365–377. Jan 22.

Bian, X.Q., Zhang, Q., Du, Z.M., Chen, J., Jaubert, J.N., 2016. A five-parameter empirical model for correlating the solubility of solid compounds in supercritical carbon dioxide. Fluid. Phase. Equilib 411, 74–80. Mar 15.

Bagheri, S., Bagheri, H., Sedghamiz, M.A., Rahimpour, M.R., 2021b. Supercritical CO_2 For biocatalysis. InGreen Sustainable Process for Chemical and Environmental Engineering and Science. Elsevier, pp. 55–72. Jan 1.

Rezaei, T., Nazarpour, V., Shahini, N., Bahmani, S., Shahkar, A., Abdihaji, M., Ahmadi, S., Shahdost, F.T., 2022. A universal methodology for reliable predicting the non-steroidal anti-inflammatory drug solubility in supercritical carbon dioxide. Sci. Rep 12 (1), 1043. Jan 20.

Bagheri, H., Hashemipour, H., Ghalandari, V., Ghader, S., 2021c. Numerical solution of particle size distribution equation: rapid expansion of supercritical solution (RESS) process. Particuology 57, 201–213. Aug 1.

Pan, L., Feng, F., Wu, J., Fan, S., Han, J., Wang, S., Yang, L., Liu, W., Wang, C., Xu, K., 2022. Demethylzeylasteral targets lactate by inhibiting histone lactylation to suppress the tumorigenicity of liver cancer stem cells. Pharmacol. Res 181, 106270. Jul 1.

Shen, W., Pei, P., Zhang, C., Li, J., Han, X., Liu, T., Shi, X., Su, Z., Han, G., Hu, L., Yang, K., 2023. A polymeric hydrogel to eliminate programmed death-ligand 1 for enhanced tumor radio-immunotherapy. ACS. Nano. Nov 21.

Xiang, J., Mlambo, R., Shaw, I., Seid, Y., Shah, H., He, Y., Kpegah, J.K., Tan, S., Zhou, W., He, B., 2023. Cryopreservation of bioflavonoid-rich plant sources and bioflavonoid-microcapsules: emerging technologies for preserving bioactivity and enhancing nutraceutical applications. Front. Nutr 10.

Li, F., Li, D., Liu, H., Cao, B.B., Jiang, F., Chen, D.N., Li, J.D., 2019. RNF216 regulates the migration of immortalized GnRH neurons by suppressing Beclin1-mediated autophagy. Front. Endocrinol. (Lausanne) 10, 12. Jan 24.

Yi, Z., Yi, Z., Huang, K., Cao, Y., Xiao, C., Li, Y., Lu, Q., Zhao, S., Luo, W., Liu, G., 2018. Propofol attenuates mast cell degranulation via inhibiting the miR-221/PI3K/Akt/Ca^{2+} pathway. Exp. Ther. Med 16 (2), 1426–1432. Aug 1.

Su, M., Hu, R., Tang, T., Tang, W., Huang, C., 2023. Review of the correlation between Chinese medicine and intestinal microbiota on the efficacy of diabetes mellitus. Front. Endocrinol. (Lausanne) 13, 1085092. Jan 25.

He, Z., Yue, C., Chen, X., Li, X., Zhang, L., Tan, S., Yi, X., Luo, G., Zhou, Y., 2023. Integrative analysis identified CD38 as a key node that correlates highly with immunophenotype, chemoradiotherapy resistance, and prognosis of head and neck cancer. J. Cancer 14 (1), 72.

Liu, Y., Li, H., Wang, X., Huang, J., Zhao, D., Tan, Y., Zhang, Z., Zhang, Z., Zhu, L., Wu, B., Chen, Z., 2023. Anti-Alzheimers molecular mechanism of icariin: insights from gut microbiota, metabolomics, and network pharmacology. J. Transl. Med 21 (1), 277. Apr 24.

Jiang, X., Yan, M., 2021. Comparing the impact on the prognosis of acute myocardial infarction critical patients of using midazolam, propofol, and dexmedetomidine for sedation. BMC. Cardiovasc. Disord 1–8. Dec; 21.

Knez, Ž., Markočič, E., Leitgeb, M., Primožič, M., Hrnčič, M.K., Škerget, M., 2014. Industrial applications of supercritical fluids: a review. Energy 77, 235–243. Dec 1.

Bagheri, H., Mohebbi, A., Amani, F.S., Naderi, M., 2022a. Application of Low Molecular Weight and High Molecular Weight Biosurfactant in Medicine/Biomedical/ Pharmaceutical industries. InGreen Sustainable Process for Chemical and Environmental Engineering and Science. Academic Press, pp. 1–60. Jan 1.

López-Periago, A., Argemí, A., Andanson, J.M., Fernández, V., García-González, C.A., Kazarian, S.G., Saurina, J., Domingo, C., 2009. Impregnation of a biocompatible polymer aided by supercritical CO_2: evaluation of drug stability and drug–matrix interactions. J. Supercrit. Fluids 48 (1), 56–63. Feb 1.

Sabegh, M.A., Rajaei, H., Esmaeilzadeh, F., Lashkarbolooki, M., 2012. Solubility of ketoprofen in supercritical carbon dioxide. J. Supercrit. Fluids 72, 191–197. Dec 1.

Bagheri, H., Hashemipour, H., Ghader, S., 2019b. Population balance modeling: application in nanoparticle formation through rapid expansion of supercritical solution. Comput. Part. Mech 721–737. Oct; 6.

Sodeifian, G., Bagheri, H., Nooshabadi, M.A., Razmimanesh, F., Roshanghias, A., 2023. Experimental solubility of fexofenadine hydrochloride (antihistamine) drug in SC-CO_2: evaluation of cubic equations of state. J. Supercrit. Fluids, 106000. May 29.

Bagheri, H., Hashemipour, H., Mirzaie, M., 2019c. Investigation on hydrodynamic and formation of nano particle by RESS process: the numerical study. J. Mol. Liq 281, 490–505. May 1.

Delma, K.L., Penoy, N., Sakira, A.K., Egrek, S., Sacheli, R., Grignard, B., Hayette, M.P., Somé, T.I., Evrard, B., Semdé, R., Piel, G., 2023. Use of supercritical CO_2 for the sterilization of liposomes: study of the influence of sterilization conditions on the chemical and physical stability of phospholipids and liposomes. Europ. J. Pharmac. Biopharmac 183, 112–118. Feb 1.

Bagheri, H., Mansoori, G.A., Hashemipour, H., 2018. A novel approach to predict drugs solubility in supercritical solvents for RESS process using various cubic EoS-mixing rule. J. Mol. Liq 261, 174–188. Jul 1.

Chapman, W.G., Gubbins, K.E., Jackson, G., Radosz, M., 1989. SAFT: equation-of-state solution model for associating fluids. Fluid Phase Equilib 52, 31–38. Dec 1.

Gross, J., Sadowski, G., 2002. Application of the perturbed-chain SAFT equation of state to associating systems. Ind. Eng. Chem. Res 41 (22), 5510–5515. Oct 30.

Gross, J., Sadowski, G., 2001. Perturbed-chain SAFT: an equation of state based on a perturbation theory for chain molecules. Ind. Eng. Chem. Res 40 (4), 1244–1260. Feb 21.

He, B., Hou, F., Ren, C., Bing, P., Xiao, X., 2021. A review of current in silico methods for repositioning drugs and chemical compounds. Front. Oncol 11, 711225. Jul 22.

Haux, J., 1999. Digitoxin is a potential anticancer agent for several types of cancer. Med. Hypotheses 53 (6), 543–548. Dec 1.

Wang, H.Y., Xin, W., Zhou, M., Stueckle, T.A., Rojanasakul, Y., O'Doherty, G.A, 2011. Stereochemical survey of digitoxin monosaccharides. ACS. Med. Chem. Lett 2 (1), 73–78. Jan 13.

Dai, W., Li, J.D., Zhao, Y., Wu, J., Jiang, F., Chen, D.N., Zheng, R., Men, M., 2020. Functional analysis of SEMA3A variants identified in Chinese patients with isolated hypogonadotropic hypogonadism. Clin. Genet 97 (5), 696–703. May.

Cai, H., Wang, H.Y., Venkatadri, R., Fu, D.X., Forman, M., Bajaj, S.O., Li, H., O'Doherty, G.A., Arav-Boger, R, 2014. Digitoxin analogues with improved anticytomegalovirus activity. ACS. Med. Chem. Lett 5 (4), 395–399. Apr 10.

https://webbook.nist.

Bagheri, H., Notej, B., Shahsavari, S., Hashemipour, H., 2022b. Supercritical carbon dioxide utilization in drug delivery: experimental study and modeling of paracetamol solubility. Europ. J. Pharmac. Sci. 177, 106273. Oct 1.

Notej, B., Bagheri, H., Alsaikhan, F., Hashemipour, H., 2023. Increasing solubility of phenytoin and raloxifene drugs: application of supercritical CO_2 technology. J. Mol. Liq, 121246. Jan 13.

Kumar, S.K., Johnston, K.P., 1988. Modelling the solubility of solids in supercritical fluids with density as the independent variable. J. Supercrit. Fluids 1 (1), 15–22. Jan 1.

Méndez-Santiago, J., Teja, A.S., 1999. The solubility of solids in supercritical fluids. Fluid. Phase. Equilib 158, 501–510. Jun 1.

Garlapati, C., Madras, G., 2010. New empirical expressions to correlate solubilities of solids in supercritical carbon dioxide. Thermochim. Acta 500 (1–2), 123–127. Mar 10.

Bartle, K.D., Clifford, A.A., Jafar, S.A., Shilstone, G.F., 1991. Solubilities of solids and liquids of low volatility in supercritical carbon dioxide. J. Phys. Chem. Ref. Data 20 (4), 713–756. Jul.

Sung, H.D., Shim, J.J., 1999. Solubility of CI disperse red 60 and CI disperse blue 60 in supercritical carbon dioxide. J. Chem. Engineer. Data 44 (5), 985–989. Sep 9.

Chrastil, J., 1982. Solubility of solids and liquids in supercritical gases. J. Phys. Chem 86 (15), 3016–3021. Jul.

Bagheri, H., Ghader, S., AbdulAmeer, S., Ahmad, N., 2023. Comprehensive study on deep eutectic solvent density based on various EoSs: SRK, PT, VTSRK, sPC-SAFT. J. Mol. Liq, 123627. Nov 20.

Sodeifian, G., Ardestani, N.S., Sajadian, S.A., Panah, H.S., 2018. Measurement, correlation and thermodynamic modeling of the solubility of Ketotifen fumarate (KTF) in supercritical carbon dioxide: evaluation of PCP-SAFT equation of state. Fluid. Phase. Equilib 458, 102–114. Feb 25.

Anvari, M.H., Pazuki, G., 2014. A study on the predictive capability of the SAFT-VR equation of state for solubility of solids in supercritical CO_2. J. Supercrit. Fluids 90, 73–83. Jun 1.

Bagheri, H., Hosseini, M.S., Zadeh, H.G., Notej, B., Fayazi, A., 2021d. A novel modification of ionic liquid mixture density based on semi-empirical equations using laplacian whale optimization algorithm. Arab. J. Chem 14 (10), 103368. Oct 1.

Bagheri, H., Karimi, N., Dan, S., Notej, B., Ghader, S., 2021e. Ionic liquid excess molar volume prediction: a conceptual comparison. J. Mol. Liq 336, 116581. Aug 15.

Bagheri, H., Ghader, S., 2017. Correlating ionic liquids density over wide range of temperature and pressure by volume shift concept. J. Mol. Liq 236, 172–183. Jun 1.

Sheikhi-Kouhsar, M., Bagheri, H., Raeissi, S., 2015. Modeling of ionic liquid+polar solvent mixture molar volumes using a generalized volume translation on the Peng-Robinson equation of state. Fluid. Phase. Equilib 395, 51–57. Jun 15.
Mokhtari, A., Bagheri, H., Ghazvini, M., Ghader, S., 2022. New mathematical modeling of temperature-based properties of ionic liquids mixture: comparison between semi-empirical equation and equation of state. Chem. Engineer. Res. Des 177, 331–353. Jan 1.
Bagheri, H., Mohebbi, A., 2017. Prediction of critical temperature, critical pressure and acentric factor of some ionic liquids using Patel-Teja equation of state based on genetic algorithm. Korean J. Chem. Engineer. 2686–2702. Oct; 34.